INTERNATIONAL JOURNAL FOR NUMERICAL METHODS IN FLUIDS, VOL. 14, 919–934 (1992)

INFLUENCE OF SKIRT RADIUS ON PERFORMANCE OF CIRCULAR CLARIFIER WITH DENSITY STRATIFICATION

SIPING ZHOU AND JOHN A. McCORQUODALE

Department of Civil and Environmental Engineering, University of Windsor, Windsor, Ontario, Canada N9B 3P4

SUMMARY

A numerical model for predicting the velocity field and suspended solids distribution in a secondary circular clarifier with density difference is evaluated. The density effects are characterized by the inlet densimetric Froude number. This study focuses on the role of the reaction baffle position in the performance of the clarifiers. For a large-radius baffle and low densimetric Froude number an important phenomenon known as the density waterfall occurs in the inlet zone of the clarifiers. This was predicted by the numerical model and confirmed by the physical model tests. This model consists of a series of conservation equations for fluid mass and momentum and sediment concentration. The turbulent stresses are calculated by use of the eddy viscosity concept and the k–ε turbulence model. The study showed that the density waterfall results in high entrainment and high recirculation. A comparison of the solids concentration distribution for a tank with a small skirt radius to that with a large skirt radius shows that small skirt radius reduces the density waterfall effect and significantly improves the clarifier performance at low densimetric Froude numbers.

KEY WORDS Secondary clarifier Numerical model Density currents Turbulence Circular tank

INTRODUCTION

Gravity sedimentation is one of the most frequently used processes in wastewater treatment. Secondary clarifiers are used to remove the settleable suspended solids created in biological treatment processes such as the activated sludge process. In these clarifiers the inlet solids concentration is usually much higher than that of primary clarifiers, which leads to density currents as well as hindered settling. A numerical model which can describe clarifier behaviour for arbitrary geometry and variable solids and hydraulic loading would be a powerful design tool that would enable the designer to make comparative analysis for different geometries under combinations of inflow rate and inlet solids concentration with various settling properties. Such a model can also be used as a diagnostic tool to guide the operation of existing clarifiers.

A classical early simple method of analysis presented by Dobbins[1] was based on the concept of overflow rate using a plug flow assumption and accounting for the effects of wall-generated turbulence on sedimentation. This simple approach fails to account for many of the hydraulic characteristics of real clarifiers. The recent progress in computational fluid dynamics and turbulent models as well as the improved capabilities of computers have made it possible to develop an advanced numerical model which can be used to consider the major factors affecting solids removal, such as: the flow pattern, including any recirculation and density currents; turbulent mixing; solids re-suspension at the bottom boundary and the quiescent settling characteristics of the particle.

0271–2091/92/080919–16$08.00

Received 21 March 1991
Revised 14 August 1991

Larsen[2] and Imam *et al.*[3] separately presented similar numerical models to simulate the settling process in rectangular clarifiers. Their models solved the streamfunction–vorticity equations by using finite difference schemes. The eddy viscosity was estimated by Prandtl mixing length theory.

Abdel-Gawad and McCorquodale[4] presented a 'strip integral' method to simulate the flow pattern and dispersion characteristics of the flow in circular primary clarifiers. The method assumes a dominant flow direction and with the use of velocity shape functions reduces the equations of motion and continuity to a set of simultaneous ordinary equations, which are solved by a Runge–Kutta method.

Celik *et al.*[5] presented a numerical model for predicting the velocity field and transient dye concentration distribution in rectangular settling tanks. They used an ADI-type finite volume method to solve the momentum equation, mass transport equation and k–ε model for 2D turbulent flow in the vertical plane of rectangular settling tanks. Their study was focused on the hydrodynamics of the neutral density flow. Transient dye concentration distributions are also calculated.

Lyn and Zhang[6] presented a two-dimensional numerical model for predicting turbulent flows in circular sediment tanks. In their model, non-orthogonal boundary-fitted non-staggered grid facilities improved the handling of boundary conditions in flows with complex geometries. The standard k–ε turbulence model provides a closure for the governing equations. The sample calculations were made for the case of a circular tank with an inlet baffle and a two-part sloping bottom divided by a sill.

In most of these studies, density effects were not fully taken into account.

DeVantier and Larock[7] presented a finite element model for stratified turbulent steady two-dimensional flow. They simulated, by direct computation, sediment-driven density currents in a circular secondary clarifier. The model consists of conservation equations for fluid mass and momentum and sediment flume, closed by a modified form of k–ε turbulence model. When they attempted to simulate the flow in the inlet zone of the clarifier, their solution was plagued by strong local numerical instabilities along the reaction baffle arising from strong local density variations.

McCorquodale *et al.*[8] presented a computer model for unsteady flow in a centre-fed circular clarifier to predict the effects of unsteady flow on clarifier performance. In their study, two cases of diurnal variation in flow at a constant MLSS concentration and a sudden increase in the MLSS were considered. The model can consider the influence of density difference on flow pattern, concentration distribution in the settling zone of the clarifier and sludge withdrawal.

In an earlier paper, Zhou and McCorquodale[9] were successful in modelling the density flow in the inlet zone as well as the settling zone. Some important phenomena were modelled and confirmed by the physical model tests, e.g. the density waterfall in the inlet zone, the influence of the waterfall on the bottom density current, flow entrainment and recirculation eddies. An explanation is given for the effect of inlet densimetric Froude number on effluent solids concentration.

The investigation reported here focuses on modelling the effects of the presence and position of a reaction baffle on the flow pattern and concentration distribution in clarifiers at low influent densimetric Froude numbers.

DEFINITION OF PROBLEM

The common type of circular clarifier has a simple cylindrical feedwell and peripheral withdrawal. For this study the flow is assumed to be axisymmetric, isothermal, density-stratified and incompressible.

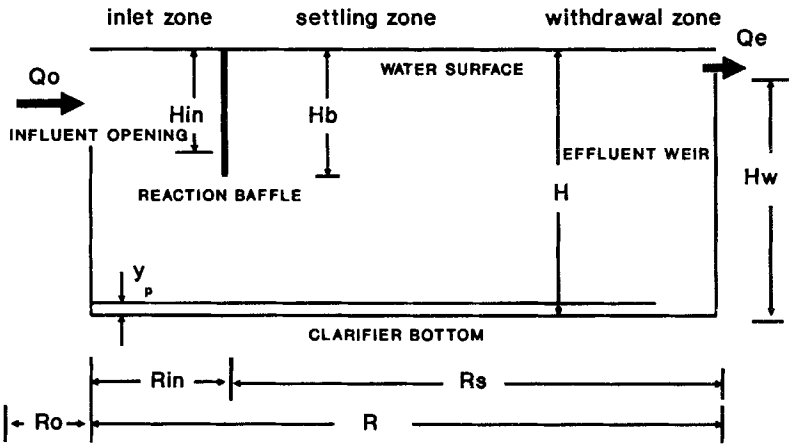

Figure 1. Definition sketch of circular clarifier

A clarifier can be divided into four different functional zones as shown in Figure 1:

(1) the inlet zone with a reaction baffle that is submerged to half the water depth
(2) the settling zone in which most of the solids removal takes place
(3) the withdrawal zone in which water flows upwards and over the outlet weir
(4) the sludge zone which typically extends from the bottom of the clarifier to just above the scraper mechanism.

In this model the primary focus of attention is zones (1)–(3). A concentration boundary condition is used to describe the relationship between the sludge zone, which was treated as a bed load layer, and the settling zone.

The controlling variables are: the clarifier radius R; the skirt radius R_{in}; the radius of the settling zone, R_s; the depth of the influent stream opening, H_{in}; the local water depth in the clarifier, H; the height of the effluent weir H_w; the height of the reaction baffle, H_b; the hydraulic loading Q_0; the influent concentration C_0; and the settling parameters.

GOVERNING EQUATIONS

The equations describing axisymmetric, two-dimensional, unsteady, turbulent and density-stratified flow in a circular setting clarifier were presented by Jensen *et al.*:[10]

continuity equation

$$\frac{\partial(ru)}{\partial r}+\frac{\partial(rv)}{\partial y}=0, \tag{1}$$

r-momentum equation

$$\frac{\partial u}{\partial t}+u\frac{\partial u}{\partial r}+v\frac{\partial u}{\partial y}=-\frac{1}{\rho}\frac{\partial p}{\partial r}+\frac{1}{r}\frac{\partial}{\partial r}\left(rv_t\frac{\partial u}{\partial r}\right)+\frac{1}{r}\frac{\partial}{\partial y}\left(rv_t\frac{\partial u}{\partial y}\right)+S_u, \tag{2}$$

y-momentum equation

$$\frac{\partial v}{\partial t}+u\frac{\partial v}{\partial r}+v\frac{\partial v}{\partial y}=-\frac{1}{\rho}\frac{\partial p}{\partial y}+\frac{1}{r}\frac{\partial}{\partial r}\left(rv_t\frac{\partial v}{\partial r}\right)+\frac{1}{r}\frac{\partial}{\partial y}\left(rv_t\frac{\partial v}{\partial y}\right)+g\frac{\rho-\rho_r}{\rho}+S_v, \tag{3}$$

where

$$S_u=\frac{1}{r}\frac{\partial}{\partial r}\left(rv_t\frac{\partial u}{\partial r}\right)+\frac{1}{r}\frac{\partial}{\partial y}\left(rv_t\frac{\partial v}{\partial r}\right)-2\frac{v_t}{r^2}u, \tag{4}$$

$$S_v=\frac{1}{r}\frac{\partial}{\partial r}\left(rv_t\frac{\partial u}{\partial y}\right)+\frac{1}{r}\frac{\partial}{\partial y}\left(rv_t\frac{\partial v}{\partial y}\right). \tag{5}$$

Symbols u and v are ensemble mean velocity components in the r- and y-direction respectively, p is the general pressure minus the hydrostatic pressure at reference density ρ_r, ρ is the fluid density, g is the gravitational acceleration and v_t is the eddy viscosity. Only differences of density ρ from some reference value are considered relevant in determining the effect of gravity.[2]

The unsteady terms of equations (2) and (3) are retained, in part to enhance computational stability and improve on iterative convergence. The steady flow solution is approached as the limit of the unsteady solution.

For density-driven flows the local fluid density is related to the local values of the sediment concentration by

$$\rho=\rho_r+C(1-S_s^{-1}), \tag{6}$$

where C is the solids concentration (same units as ρ) and S_s is the specific gravity of solid particles.

The convection–diffusion equation, which describes the concentration distribution of suspended solids, can be derived by applying the principle of conservation of mass to a differential volume element within the flow. For a two-dimensional, unsteady mean flow the concentration equation is[4]

$$\frac{\partial C}{\partial t}+u\frac{\partial C}{\partial r}+v\frac{\partial C}{\partial y}=\frac{1}{r}\frac{\partial}{\partial r}\left(rv_{sr}\frac{\partial C}{\partial r}\right)+\frac{1}{r}\frac{\partial}{\partial y}\left(rv_{sy}\frac{\partial C}{\partial y}+rV_sC\right), \tag{7}$$

in which v_{sr} is the eddy diffusivity of suspended solids in the r-direction, v_{sy} is the eddy diffusivity of suspended solids in the y-direction and V_s is the particle-settling velocity (positive downwards). By using the Reynolds analogy between mass transport and momentum transport, the sediment diffusion coefficient is related to v_t by

$$v_{sr}=\frac{v_t}{\sigma_{sr}}, \qquad v_{sy}=\frac{v_t}{\sigma_{sy}}, \tag{8}$$

in which σ_{sr} and σ_{sy} are the Schmidt numbers in the r- and y-direction respectively.

TURBULENCE MODEL

The eddy viscosity is calculated from the k–ε turbulence model,[11] which relates v_t to the turbulence kinetic energy k and the turbulence dissipation rate ε, i.e.

$$v_t=C_\mu\frac{k^2}{\varepsilon}. \tag{9}$$

The distributions of k and ε are calculated from the following semi-empirical transport equations:

$$\frac{\partial k}{\partial t}+u\frac{\partial k}{\partial r}+v\frac{\partial k}{\partial y}=\frac{1}{r}\frac{\partial}{\partial r}\left(r\frac{\nu_t}{\sigma_k}\frac{\partial k}{\partial r}\right)+\frac{1}{r}\frac{\partial}{\partial y}\left(r\frac{\nu_t}{\sigma_k}\frac{\partial k}{\partial y}\right)+P-\varepsilon, \tag{10}$$

$$\frac{\partial \varepsilon}{\partial t}+u\frac{\partial \varepsilon}{\partial r}+v\frac{\partial \varepsilon}{\partial y}=\frac{1}{r}\frac{\partial}{\partial r}\left(r\frac{\nu_t}{\sigma_\varepsilon}\frac{\partial \varepsilon}{\partial r}\right)+\frac{1}{r}\frac{\partial}{\partial y}\left(r\frac{\nu_t}{\sigma_\varepsilon}\frac{\partial \varepsilon}{\partial y}\right)+C_1\frac{\varepsilon}{k}P-C_2\frac{\varepsilon^2}{k}, \tag{11}$$

in which P is the production of turbulent energy by the mean velocity gradients, i.e.

$$P=\nu_t\left[2\left(\frac{\partial u}{\partial r}\right)^2+2\left(\frac{\partial v}{\partial y}\right)^2+2\left(\frac{u}{r}\right)^2+\left(\frac{\partial u}{\partial y}+\frac{\partial v}{\partial r}\right)^2\right]. \tag{12}$$

The standard k–ε model constants $C_1=1{\cdot}44$, $C_2=1{\cdot}92$ and $C_\mu=0{\cdot}09$ as well as the turbulent Prandtl numbers for k and ε, $\sigma_k=1{\cdot}0$ and $\sigma_\varepsilon=1{\cdot}30$, were used.[11] In the current study the buoyancy correction terms involving the flux Richardson number in the k–ε model were omitted as a first approximation.[12]

BOUNDARY CONDITIONS

Inlet boundary

A uniform, parallel inlet flow was imposed, with radial velocity $u=u_0$ and vertical velocity $v=0$, inlet $k=0{\cdot}2u_0^2$, $\varepsilon=C_\mu^{3/4}k^{3/2}/l_m$, mixing length $l_m=C_\mu(0{\cdot}5H_{in})$ and $C=C_0$ over the inlet area per unit curvature (R_0H_{in}).

Free surface boundary

The rigid lid approximation is made and the free surface boundary is treated as a symmetry surface. The presence of a free surface reduces the turbulent length scale and the following empirical boundary condition of Celik and Rodi[13] was used.

$$\varepsilon=\frac{k^{3/2}}{0{\cdot}43H}. \tag{13}$$

For sediment concentration C the free surface is considered to be a non-penetrating boundary,[3] i.e.

$$\frac{\partial C}{\partial y}=-\frac{V_s}{\nu_{sy}}C. \tag{14}$$

Baffle and vertical weir

These were treated as reflecting boundaries with $\partial C/\partial r=0$.

Outlet boundary

The values imposed at the outlet are extrapolated from computed near-outlet values, with the restriction that overall continuity is always satisfied.

Solid boundaries

The standard k–ε model treatment using wall functions assuming locally parallel, equilibrium turbulent wall flow was used. Thus near-wall velocities are determined from a local application of log-law, and near-wall k and ε from assumptions of local equilibrium.

Bed boundary

For a realistic simulation of the concentration profiles it is essential to develop a correct bed boundary condition for the sediment concentration under non-equilibrium conditions. Sediment transport in settling tanks can be treated in two layers, i.e. a bed load layer that contains settled matter with high concentration and a suspended load layer. Unfortunately, there is no distinct boundary between the two layers. As an approximate treatment and for convenience the computational position of the suspension boundary is matched to that of the k–ε model. The thickness of the bed load layer is assumed to be y_p and the thickness of the suspended load layer is $H - y_p$. The exchanges of sediment particles between the bed load layer and the suspended load layer for non-equilibrium situations can be described by[14]

$$C_p = C \Big/ \left(1 - k_r \frac{V_s - V_p}{\nu_{sy}/\Delta y} \right), \tag{15}$$

where $\nu_{sy} = \nu_t/\sigma_{sy}$, C_p is the boundary value of sediment concentration, V_p is the vertical velocity component on the bottom boundary layer at $y = y_p$ and the scouring parameter k_r is restricted to the range $0 < k_r < \min(1, (\nu_{sy}/\Delta y)/(V_s - V_p))$ for net deposition and $1 < k_r < (\nu_{sy}/\Delta y)/(V_s - V_p)$ for net scouring. The term $(V_s - V_p)/(\nu_{sy}/\Delta y)$ is the ratio of the resultant settling flux downwards to the turbulent flux upwards.

SETTLING VELOCITY OF SUSPENDED SOLIDS

The works of Larsen,[2] Imam *et al.*[3] and Takacs and Nolasco[15] have identified that the quiescent settling characteristics of particles is one of the major factors affecting solids removal. In 1987 a series of batch-settling tests were conducted at the Metropolitan Seattle West Point Treatment Plant.[16] The results of these tests are summarized in Figure 2(a). The double-exponential formula of Takacs and Nolasco[15] is one of the many equations that can be fitted to these data:

$$V_s = V_0(e^{-K(C - C_{min})} - e^{-K1(C - C_{min})}), \tag{16}$$

where V_0 is the Stokes velocity of an individual particle, K is the floc-settling parameter, $K1$ is the colloids-settling parameter and C_{min} is the minimum attainable suspended solids concentration. The main advantage of this formula relative to the single-exponential formula is that it allows for a lower settling velocity in a low-solids-concentration environment in which the remaining particle diameter is usually small. Values of $K = 0{\cdot}0005$, $K1 = 0{\cdot}015$–$0{\cdot}030$ and $C_{min} = 0{\cdot}002C_0$ give reasonable agreement with experimental data as shown in Figure 2(b).

SOLUTION PROCEDURES

In the numerical model the dependent variables are u, v, p, c, k, ε, V_s and ρ. The density ρ is calculated as a function of C. The partial differential equations were solved by the finite difference procedure of Patankar and Spalding.[17,18] Equations (1)–(3), (7), (10) and (11) can be presented in

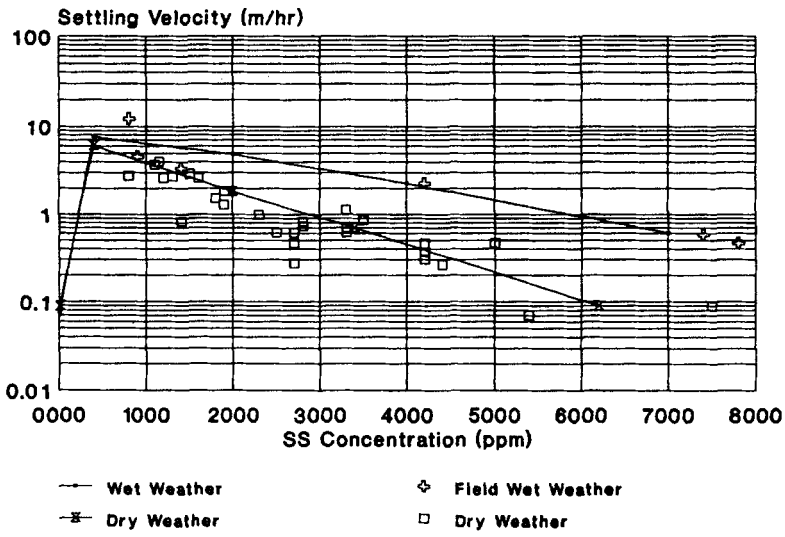

Figure 2(a). Experimental data of settling velocity

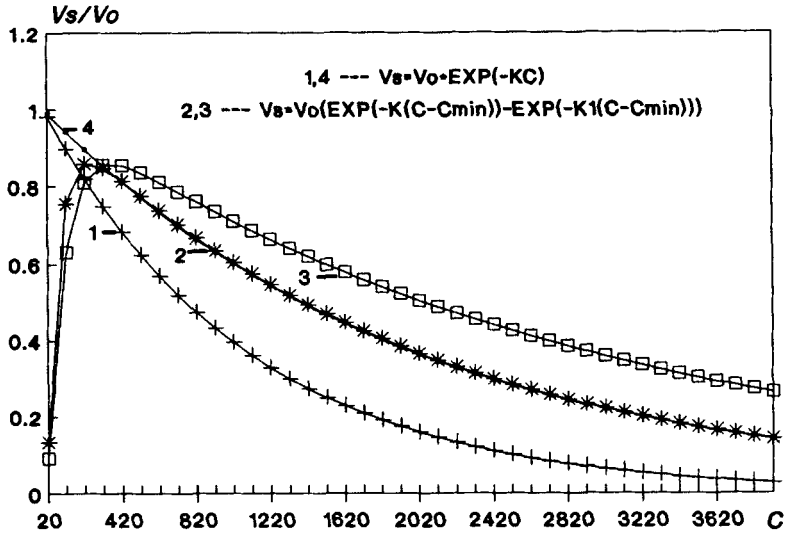

Figure 2(b). Presentation of settling velocity models

the general form

$$\frac{\partial \varphi}{\partial t}+u\frac{\partial \varphi}{\partial r}+v\frac{\partial \varphi}{\partial y}=\frac{1}{r}\frac{\partial}{\partial r}\left(r\frac{\nu_t}{\sigma_\varphi}\frac{\partial \varphi}{\partial r}\right)+\frac{1}{r}\frac{\partial}{\partial y}\left(r\frac{\nu_t}{\sigma_\varphi}\frac{\partial \varphi}{\partial y}\right)+S_\varphi. \tag{17}$$

A 'staggered' grid is constructed in the (r, y) co-ordinate system as shown in Figures 2(c) and 2(d); the dependent variables are to be computed for all the grid points. Figure 2(d) shows a small volume element surrounding each grid point. The finite difference equations are derived by

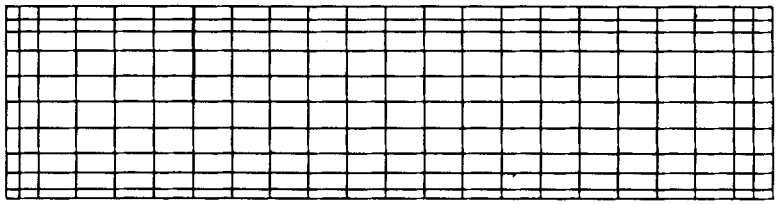

Figure 2(c). Computational domain

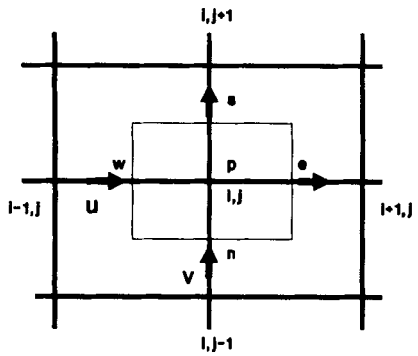

Figure 2(d). Grid elements for finite difference calculations (the control volume for concentration C and pressure p consists of thin lines)

integrating the partial differential equations over the control volume. The resulting algebraic equations at grid points can be written in the form

$$(A_p - S_p)\varphi_{i,j} = A_w\varphi_{i-1,j} + A_e\varphi_{i+1,j} + A_s\varphi_{i,j-1} + A_n\varphi_{i,j+1} + B, \tag{18}$$

where the coefficients A_p to A_n are functions of the mass fluxes across the face of the control volume as described elsewhere[18] and

$$B + S_p\varphi_{i,j} = (r\Delta r\Delta y)S_\varphi. \tag{19}$$

These equations are solved by a line-by-line iteration method.

For low-densimetric-Froude-number situations, strong numerical instabilities may be encountered in the iteration procedure since the excess density body force $g(\rho - \rho_r)/\rho$ appears in the momentum equation. To avoid divergence of the iterative algorithm, a relatively low underrelaxation coefficient (0·15–0·2) was adopted in the iteration procedure for the momentum equation and the unsteady model was used. In the present numerical model for simulation of flow in secondary sedimentation tanks, the density term is the main link between the flow equations and the sediment transport equations. In order to slow down the rate of change of density ρ in the interactive process so that it matches the rate of change of pressure field, an underrelaxation procedure for ρ was used as follows:

$$\rho = \alpha\rho_{new} + (1 - \alpha)\rho_{old}, \tag{20}$$

where $\alpha = 0{\cdot}1$–$0{\cdot}2$. Furthermore, with this formula an appropriate underrelaxation of the source term involving the buoyancy force in the momentum equation (3) is helpful in reducing numerical oscillation and ensuring iterative convergence.

For a given time step and at each iteration an estimate of the pressure field p is inserted into the momentum equations, but in this procedure the velocity field may not satisfy continuity; therefore corrections to the pressure field are calculated which bring the velocity field into conformity with continuity. In this iterative procedure the unsteady terms for all dependent variables remain unchanged until the start of the new time step.

RESULTS AND DISCUSSION

Clarifier hydrodynamics

Figure 3 shows the velocity field for a neutral density situation with an inflow $Q_0 = 0{\cdot}3\ \mathrm{m^3\,s^{-1}}$, $H = 3{\cdot}0$ m, a return activated sludge ratio of zero and $R_{in}/H = 1{\cdot}0$. The influent, after impinging on the reaction baffle at A, is deflected downwards to the tank bottom. The flow splits at B on the bottom near the section of the reaction baffle, producing a recirculation eddy at C occupying most of the inlet zone and in outward bottom current under the submerged baffle lip (A′). This impingement with the baffle and the sudden decrease in velocity bring about a large loss of kinetic energy.

Using the same inlet flow rate ($0{\cdot}3\ \mathrm{m^3\,s^{-1}}$) but with $C_0 = 750\ \mathrm{mg\,l^{-1}}$ (densimetric Froude number $Fr = 0{\cdot}35$), the model gave the flow pattern shown in Figure 4(a) for $R_{in}/H = 1{\cdot}0$. The added density of the influent caused the inflow to dive towards the bed without impinging on the baffle. The flow split point B moved upstream compared to the position in the neutral case (Figure 3). A strong bottom density current formed. The inlet recirculation zone C is very small. However, the diving plume, owing to its high entrainment, draws fluid from the settling zone, thus causing a counterflow under the reaction baffle at A′ and a large recirculation zone in the upper part of the inlet zone A. Since the inflow jet does not impinge on the reaction baffle, the loss of kinetic energy is low and the potential energy of the influent produces a high downward velocity; this results in a high-velocity horizontal density current which is much shallower than the bottom current in the neutral case.

A physical model was used to confirm the existence of the diving plume or waterfall predicted by the numerical model. The physical model also showed that the entrainment by the waterfall caused a strong counterflow in the inlet zone. Figure 5(a) shows the impingement on the baffle, the resulting bottom current and the inlet recirculation zone for neutral density. Figure 5(b) shows the corresponding flow pattern for density flow; the waterfall effect and the shallower bottom current are evident. The density waterfall was produced from the neutral initial state by decreasing the influent temperature, giving a densimetric Froude number of about 0·35.

A number of researchers have observed the solids-cascading phenomenon in clarification of activated sludge in physical models and field tanks.[19–22] Figure 5(c), presented by Augustus

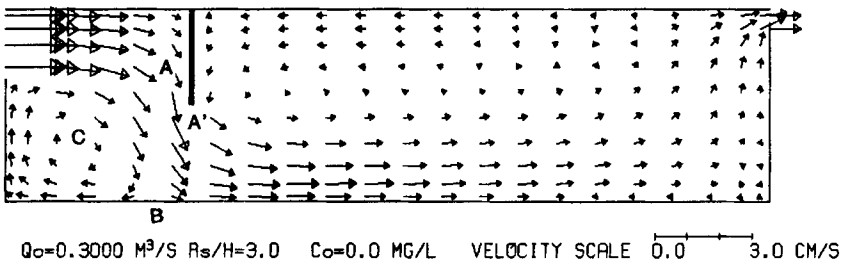

Figure 3. Flow pattern in circular clarifier for neutral density situation ($R_{in}/H = 1{\cdot}0$)

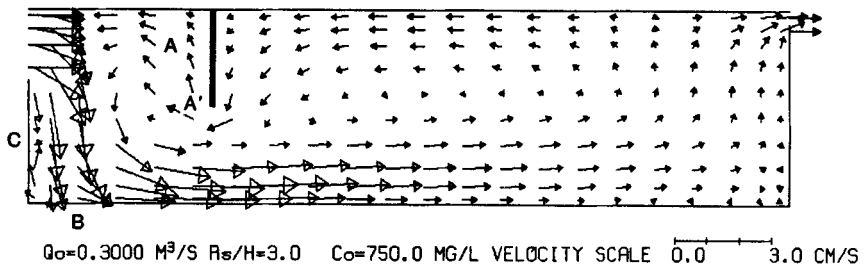

Figure 4(a). Predicted velocity field: clarifier with a reaction baffle and large skirt radius ($R_{in}/H = 1{\cdot}0$)

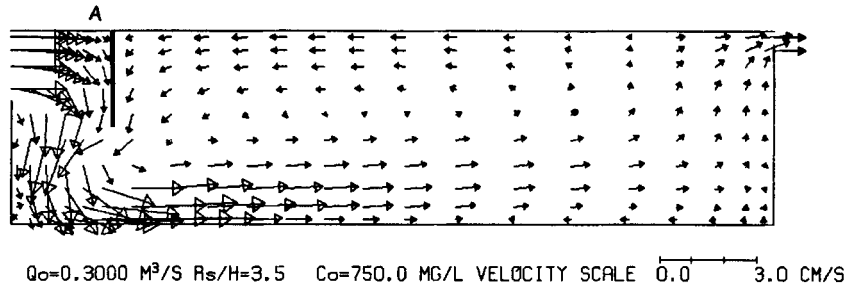

Figure 4(b). Predicted velocity field: clarifier with a reaction baffle and small skirt radius ($R_{in}/H = 0{\cdot}53$)

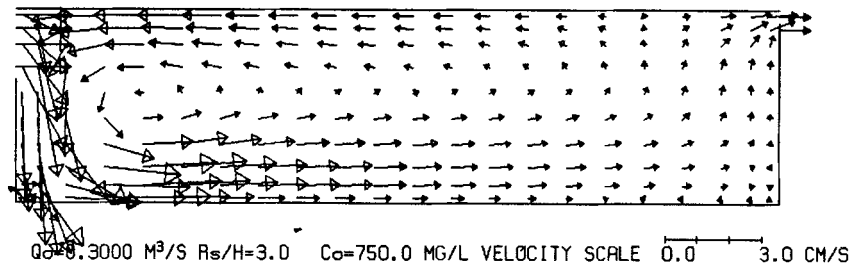

Figure 4(c). Predicted velocity field: clarifier with no reaction baffle

et al.,[22] shows a typical flow pattern associated with a density waterfall. It has been suggested that reducing the cascading effect and using the upper portion of the centre feedwell to dissipate kinetic energy can improve clarifier performance.[22]

Effect of baffle radius on hydrodynamics

Studies by McCorquodale[23] revealed the importance of the inlet reaction baffle in dissipating the kinetic energy of the incoming flow and reducing short-circuiting, particularly in the case of a buoyant density current. Some researchers[22] have indicated that the location of the reaction baffle has a pronounced effect on the nature of the flow through the clarifier; however, the design standards for the cylindrical feedwell diameter do not reflect this concern. Most primary and

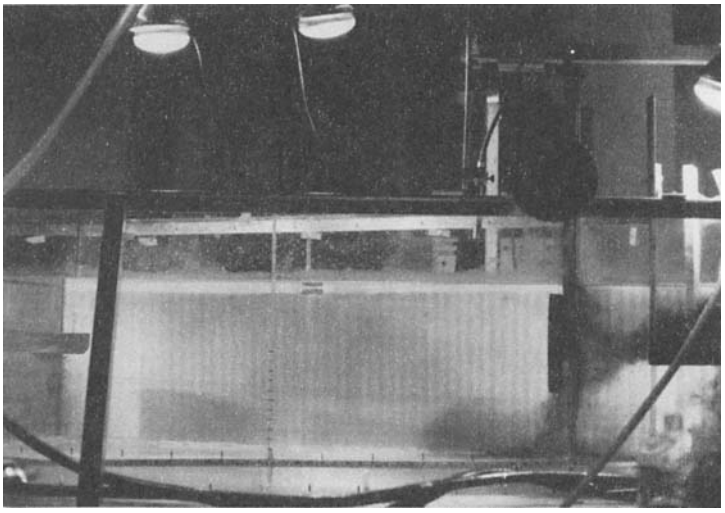

Figure 5(a). Flow impinging on reaction baffle for neutral density influent

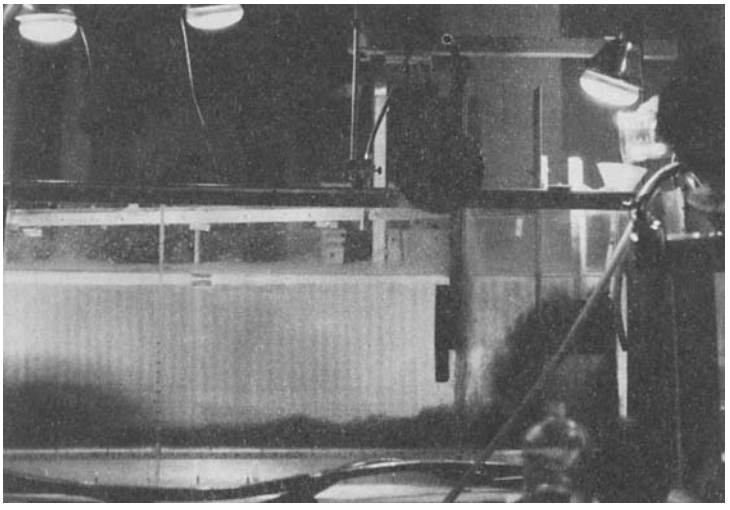

Figure 5(b). Density waterfall phenomenon in clarifier with reaction baffle

secondary clarifiers have a simple cylindrical feedwall diameter equal to 20%–30% of the tank diameter. Some manufacturers advise that feedwell diameters should not exceed 10·7–13 m regardless of the tank size.[22] Gurnham[24] suggests that baffles serve a useful purpose in dissipating the inlet velocity and should be placed 0·6–1 m in front of the inlet parts for best results.

To illustrate the effect of the feedwell radius on the flow pattern, two baffle radii were considered, namely $R_{in}/H = 1{\cdot}0$ and 0·53, with the same hydraulic and solids loadings. As shown in Figures 4(a) and 4(b), the influent jet does not impinge on the baffle at $R_{in}/H = 1{\cdot}0$ but impinges strongly at $R_{in}/H = 0{\cdot}53$ for the case of low densimetric Froude number ($Fr = 0{\cdot}35$). The small

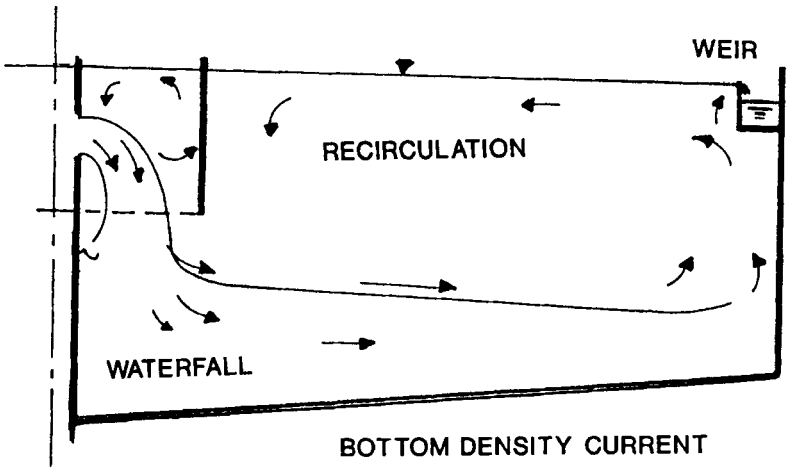

Figure 5(c). Solids-cascading phenomenon in clarification of activated sludge (from Reference 22)

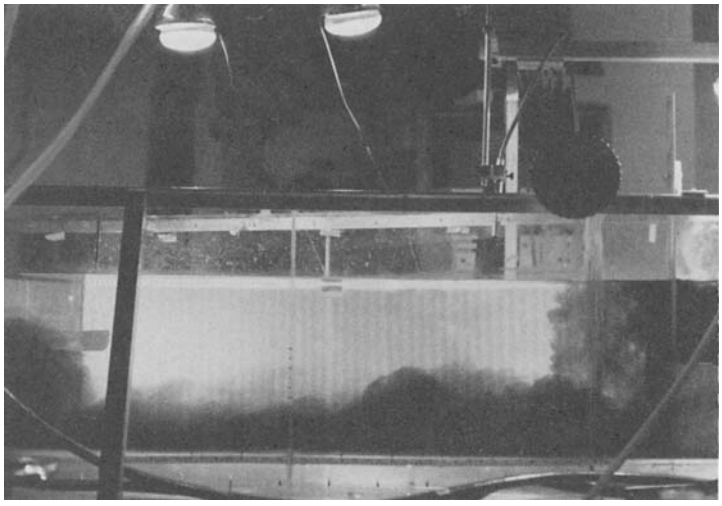

Figure 5(d). Density waterfall phenomenon in clarifier with no baffle

feedwell reduced the entrainment of fluid in the waterfall, thus eliminating the recirculation eddies at A compared to the large-feedwell case. For the large feedwell the large eddy restricted the space for active downward flow, with the result that the downward velocity was increased. The smaller-radius baffle resulted in a 13% decrease in the maximum downward velocity. In addition, the flow impinging on the smaller-radius baffle would dissipate more kinetic energy than the non-impinging flow on the large-radius baffle.

The performance of the feedwell depends very strongly on the densimetric Froude number. At the low densimetric Froude numbers considered in this paper a small feedwell is preferred, while at high Froude numbers (including neutral density flow) a larger feedwell radius would give better results.

There are two other important hydrodynamic and related factors that affect the solids distribution in a secondary clarifier, i.e. the strength of the bottom density current and the upward current in the withdrawal zone. Based on a study of physical models in Morgantown, NC, Crosby[20] observed that the downward and radial flow of liquid from the influent to the effluent walls often creates a 'rebound' at the clarifier wall. The upward velocities at the wall can carry some of the bottom solids up and into the effluent launders. Crosby[20] used an additional baffle at mid-radius extending from the floor upwards to mid-depth to break up the radial density current; suspended solids data collected after the ring baffle installation showed a reduction of 38% in effluent concentration.

The dimensionless bottom current flow rate and the dimensionless upward current flow rate in the downstream zone of the clarifier are plotted against radial distance and vertical distance respectively in Figures 6 and 7. The maximum ratio of the bottom current flow rate to the inflow rate decreased from 1·68 to 1·45, a 14% improvement, when the reaction baffle was moved from $R_{in}/H = 1{\cdot}0$ to 0·53. As indicated in Figure 7, there was a corresponding 8·4% decrease in upward flow in the withdrawal zone when R_{in}/H was reduced from 1·0 to 0·53. The strength of the rebound phenomenon is directly related to the strength of the bottom current by continuity and momentum relationships.

Figure 4(c) shows the velocity field of the clarifier with no reaction baffle and the same hydraulic loading and inlet concentration as the previous two cases. Although there is no baffle installed upstream of the clarifier, the inlet surface flow still plunged towards the bottom of the clarifier and a strong bottom density current was formed. The surface return flow and the flow entrainment near the front end of the clarifier were considerably higher than for cases with a baffle. As shown in Figure 6, the maximum ratio of the bottom density current flow rate to the inlet flow rate was 2·19 at the section $r/R = 0{\cdot}20$, i.e. 30% higher than for $R_{in}/H = 1{\cdot}0$ and 51% higher than for $R_{in}/H = 0{\cdot}53$. However, it can been seen that the difference between the cases with no baffle and with a baffle of $R_{in}/H = 1{\cdot}0$ was mostly restricted in the inner zone of the clarifier ($r/R < 0{\cdot}5$), so that the upward flow rate in the downstream zone of the clarifier was only slightly

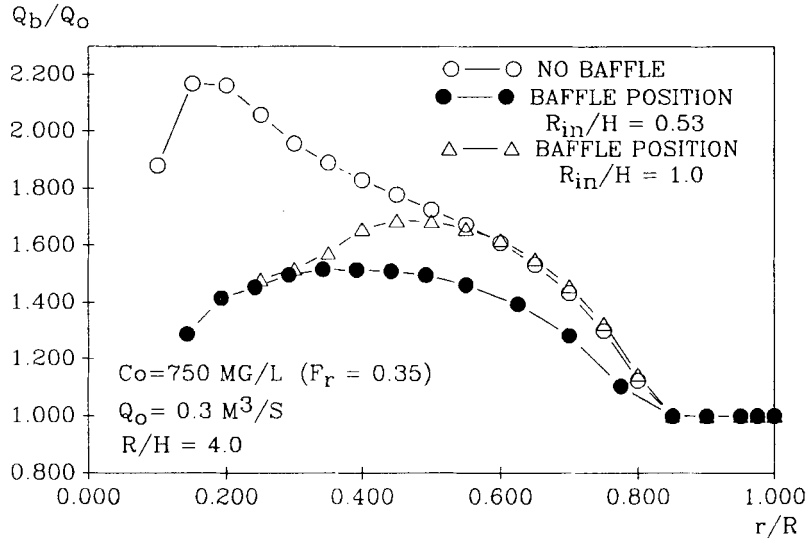

Figure 6. Strength of bottom density current for clarifiers with different skirt radius and no baffle

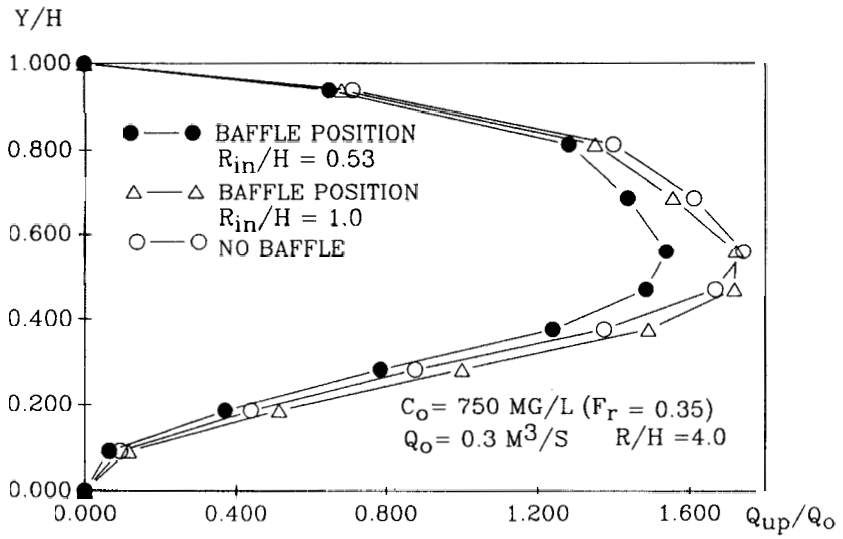

Figure 7. Strength of upward flow current for clarifiers with different skirt radius and no baffle

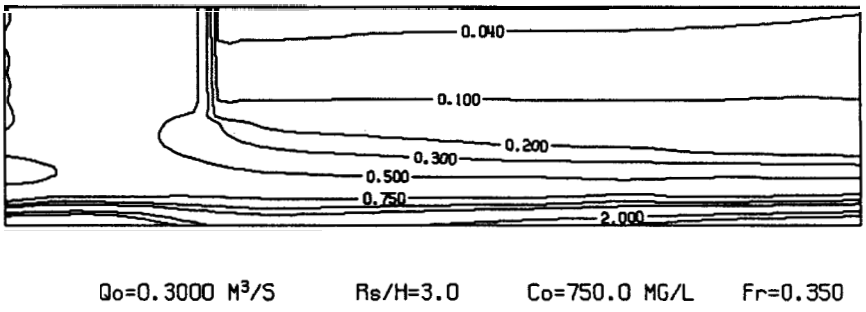

Figure 8. Contour plot of solids concentration in clarifier with large skirt radius ($R_{in}/H = 1{\cdot}0$)

different. A possible explanation for this is that in both cases (no baffle and $R_{in}/H = 1{\cdot}0$ with low Froude number) there is no flow impingement on a baffle and there is a very low force to reduce the inlet momentum flux. Thus in both cases the momentum in the radial direction at the wall was higher than for the case where the inflow impinged on the reaction baffle.

Two different physical model tests for the cases with and without a reaction baffle are shown in Figures 5(b) and 5(d) respectively. By comparing the dye concentrations for the cool influent near the reaction baffle position, it is evident that the flow entrainment in the clarifier with no baffle is much stronger than that with a baffle.

Effect of baffle radius on solids distribution

Contour plots of predicted suspended solids concentration are given in Figures 8 and 9 for $R_{in}/H = 1{\cdot}0$ and 0·53 respectively. It can be seen that the concentration contour lines for 40 and 100 $mg\,l^{-1}$ are shifted downwards when the smaller skirt is used; the effluent suspended solids concentration showed a reduction from 34 to 26 $mg\,l^{-1}$, i.e. a 22% improvement, for the smaller skirt radius compared to the larger skirt radius.

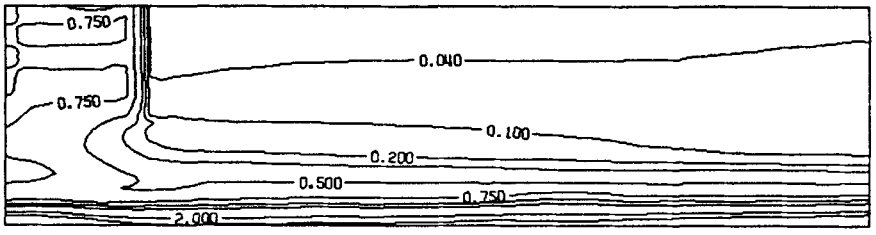

Figure 9. Contour plot of solids concentration in clarifier with small skirt radius ($R_{in}/H = 0{\cdot}53$)

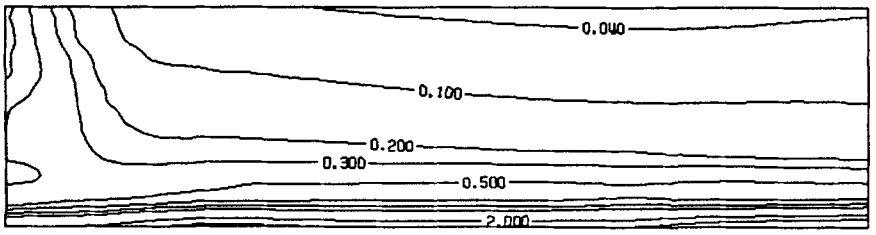

Figure 10. Contour plot of solids concentration in clarifier with no reaction baffle

Figure 10 shows the solids concentration contours for the case with no baffle, with the same low densimetric Froude number as the cases represented in Figures 8 and 9. It is evident from Figures 8 and 10 that the concentration of suspended solids is almost identical in the downstream zone for the cases of no baffle and a skirt radius $R_{in}/H = 1{\cdot}0$. This illustrates the importance of the rebound phenomenon on solids distribution and effluent concentration. The greater the rebound, the stronger will be the upflow and the higher will be the concentration of solids in the effluent.

CONCLUSIONS

The dominant flow features of density flow in circular clarifiers with and without reaction baffles have been captured by a numerical model and confirmed with a physical model. As a simulation tool, the numerical model provides an alternative method for evaluation of various secondary clarifier designs.

The numerical model was applied to clarifiers with various skirt radii. The results suggest that clarifiers with low densimetric Froude numbers perform better with smaller skirt radius. As the Froude number increases, the skirt radius for best performance also increases. It was found that a skirt with large radius at low densimetric Froude number did not achieve inflow impingement and thus could not effectively reduce the inlet momentum flux. The ultimate effect was an increase in the rebound strength at the effluent weir and consequently an increase in the outflow of solids.

ACKNOWLEDGEMENT

This research was supported by a grant from the Natural Sciences and Engineering Research Council of Canada.

REFERENCES

1. W. E. Dobbins, 'Effect of turbulence on sedimentation', *Trans. ASCE*, **109**, 629–656 (1944).
2. P. Larsen, 'On the hydraulics of rectangular settling basins, experimental and theoretical studies', *Department of Water Resources Engineering, Lund Institute of Technology, Lund University, Rep. No. 1001*, 1977.
3. E. Imam, J. A. McCorquodale and J. K. Bewtra, 'Numerical modelling of sedimentation tanks', *ASCE, J. Hydraul. Eng.*, **109**, 1740–1754 (1983).
4. S. M. Abdel-Gawad and J. A. McCorquodale, 'Strip integral method applied to settling tanks', *J. Hydraul. Eng.*, **110**, 1–17 (1984).
5. I. Celik, W. Rodi and A. Stamou, 'Prediction of hydrodynamic characteristics of rectangular settling tanks', *Proc. Int. Symp. on Refined Flow Modelling and Turbulence Measurements*, Iowa City, IA, 1985, pp. 641–651.
6. D. A. Lyn and Z. Zhang, 'Boundary-fitted numerical modelling of sedimentation tanks', *Proc. 23rd IAHR and AIRH*, Ottawa, 1989, pp. A331–A338.
7. B. A. DeVantier and B. E. Larock, 'Modeling sediment-induced density current in sedimentation basins', *J. Hydraul. Eng.*, **113**, 80–94 (1987).
8. J. A. McCorquodale, E. M. Yuen, R. W. Samstag and Z. Vitasovic, 'Numerical modelling of circular secondary clarifiers', *25th Symp. on Water Pollution Research*, Burlington, Ontario, 1990.
9. S. Zhou and J. A. McCorquodale, 'A numerical model for a circular clarifier', *Research Report*, University of Windsor, Ontario, 1990. IRI06–90
10. D. E. Jensen, D. B. Spalding, D. G. Tatchell and A. S. Wilson, 'Computation of structure of flames with recirculating flow and radial pressure gradients', in D. B. Spalding (ed.), *Numerical Prediction of Flow, Heat Transfer, Turbulence and Combustion*, Pergamon, Oxford/New York, 1979. pp. 368–377.
11. W. Rodi, 'Turbulence models and their application in hydraulics, a state-of-the art review', Book publication of International Association for Hydraulic Research, Delft, Netherlands, 1980.
12. B. A. DeVantier and B. E. Larock, 'Modeling a recirculation density-driven turbulent flow', *Int. j. numer methods fluids*, **6**, 241–253 (1986).
13. I. Celik and W. Rodi, 'Sediment transport under steady, non-equilibrium situations', in W. Bechteler (ed.), *Transport of Suspended Solids in Open Channels*, Balkema, Rotterdam/Boston, MA, 1986, pp. 97–100.
14. T. Takamatsu, M. Naito, S. Shiba and Y. Ueda, 'Effect of deposit resuspension of settling basins', *ASCE, J. Environ. Eng. Div.*, **100**, 883–903 (1974).
15. I. Takacs and D. Nolasco, 'Notes to the Vitasovic settler', personal communication, 1989.
16. R. W. Samstag, D. F. Dittmar and Z. Vitasovic, 'Studies in activated sludge sedimentation', *Proc. ASCE Civ. Eng. Environ., Eng. Spec. Conf. 39*, Vancover, 1988.
17. S. V. Patankar and D. B. Spalding, 'A calculation procedure for heat, mass and momentum transfer in three-dimensional parabolic flow', *Int. J. Heat Mass Transfer*, **15**, 1787 (1972).
18. S. V. Patankar, *Numerical Heat Transfer and Fluid Flow*, McGraw-Hill, New York, 1980.
19. J. H. Robinson, 'A study of density current in final sedimentation basins', *M.S. Thesis*, University of Kansas, Lawrence, 1974.
20. R. M. Crosby, 'Hydraulic characteristics of activated sludge-secondary clarifiers', *EPA 600/2-84-131, NTIS No. PB-84-229665*, U.S. EPA, Municipal and Environmental Research Laboratories, Cincinnatti, OH, 1984.
21. K. L. Murphy, 'Tracer studies in circular sedimentation basins', *Proc. 39th Industrial Waste Conf.*, Purdue Univ. West Lafayette, 1984 Ind., 374.
22. M. Augustus, J. M. Baler, C. Chen, G. T. Daigger, G. T. Griffith and R. J. TeKippe, *Clarifier Design*, Water Pollution Control Federation, Lancaster Press, 1985. Printed in U.S.A.
23. J. A. McCorquodale, 'Hydraulic study of the circular settling tanks at the West Windsor pollution control plant', University of Windsor, Ontario, 1976.
24. C. F. Gurnham *Principles of Industrial Waste*, Wiley, New York, 1955.
25. T. R. Camp, 'Sedimentation and the design of settling tanks', *Trans. ASCE*, **111**, 895–936 (1946).